Contrib Mineral Petrol (1995) 122: 174–190

Dmitri A. Ionov · Suzanne Y. O'Reilly
Igor V. Ashchepkov

Feldspar-bearing lherzolite xenoliths in alkali basalts from Hamar-Daban, southern Baikal region, Russia

Received: 20 March 1995 / Accepted: 26 June 1995

Abstract Lherzolite xenoliths in Miocene to Pleistocene basalts from five sites in the Hamar-Daban range in southern Siberia provide sampling of the mantle close to the axis of the Baikal rift. These anhydrous spinel lherzolites commonly have foliated fabrics and spongy rims around clinopyroxene, and many contain accessory feldspar. The feldspar occurs in reaction zones adjacent to spinel and orthopyroxene (where it appears to have been formed by the reaction: spl+opx+cpx+fluid $\rightarrow$ fs+ol) and less commonly as thin, irregular veins. The feldspars have variable compositions but are generally alkali-rich; their K_2O content ranges from 0.3 to 11.2% and is much higher than in plagioclase from orogenic lherzolites (usually $<0.1\%$ K_2O). The temperature range for the Hamar-Daban xenolith suite (950–1010° C) is more restricted than for spinel peridotite xenoliths from other occurrences in the Baikal area. The feldspar-bearing lherzolites yield equilibration temperatures similar to or slightly lower than feldspar-free ones. The majority of the Hamar-Daban lherzolites are fertile and clinopyroxene-rich, as for most other occurrences in the Baikal region. Trace element compositions of selected xenoliths and their clinopyroxenes were determined by ICP-MS, INAA and proton microprobe. Feldspar-bearing xenoliths are enriched in alkalies indicating that feldspar formation is associated with addition of material and is not simply due to isochemical phase changes. Most xenoliths and their clinopyroxenes studied are depleted in light REE and have contents of Sr, Zr and Y common for fertile or moderately depleted mantle peridotites. Few are moderately enriched in LREE, Sr, Th and U. Sr-Nd isotope compositions of clinopyroxenes indicate long-term depletion in incompatible elements similar to unmetasomatised xenoliths from other occurrences south and east of Lake Baikal. The formation of feldspar and of spongy aggregates after clinopyroxene, and the enrichment in alkalies appear to be recent phenomena related to infiltration of an alkali-rich, H_2O-poor fluid into spinel peridotites.

D.A. Ionov (✉) · S.Y. O'Reilly
Centre for Petrology and Lithospheric Studies, School of Earth Sciences, Macquarie University, Sydney, NSW 2109, Australia

I.V. Ashchepkov
United Institute of Geology, Mineralogy and Geophysics, Novosibirsk 630090, Russia

Editorial responsibility: J. Hoefs

Introduction

A large number of mantle xenolith occurrences are known in the Baikal rift zone (BRZ) in southern Siberia, Russia (Kiselev et al. 1979; Ashchepkov 1991). Basaltic rocks in the BRZ commonly occur outside the basins of the rift system. Xenolith occurrences nearest to the rift axis are on the northern slope of the Hamar-Daban Range south of Lake Baikal (Fig. 1). [A number of geographic maps provide an alternative transcription "Khamar-Daban" that does not properly render that name from Russian or Buryat (Mongolian) into English]. Wet chemical and microprobe analyses of some xenoliths from that area have been published in Russian literature (Kiselev et al. 1979; Ashchepkov 1991). We present here microstructural, major element, trace element and isotopic data for a suite of lherzolite xenoliths collected at several sites in northwestern Hamar-Daban (Fig. 1). An unusual feature of the Hamar-Daban xenoliths is common occurrence of accessory feldspar that is very rare in other peridotite xenolith suites worldwide. The major aim of this paper is to address the origin of feldspar in the source region of the xenoliths. Another aim is to provide direct information of the composition of the uppermost mantle in the vicinity of a continental rift.

Geological setting and sampling sites

The Hamar-Daban range stretches along the southern shore of Lake Baikal from the Selenga river in the east to Lake Hubsugul in northern Mongolia in the west. Ceno-

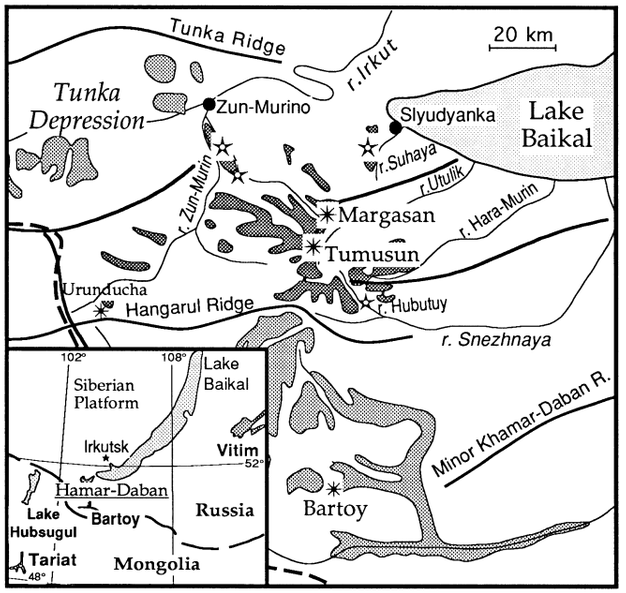

Fig. 1 Location map. Volcanic fields (after Kiselev et al. 1979) and xenolith occurrences southwest of Lake Baikal. The Hamar-Daban volcanic field is shown with *thicker fill* (the basalts may not cover the whole area shown, but in places occur as eroded relics of former continuous lava flows). Sampling sites are shown as *large stars*, other known xenolith occurrences as *small stars*. *Inset* shows location of major Cenozoic volcanic fields south and east of Lake Baikal

zoic basalts occur in the western section of the Hamar-Daban range, south and southwest of southern tip of Lake Baikal (Fig. 1). The volcanic activity was most widespread and abundant in the Miocene and eruptions continued locally until the Pleistocene. The Oligocene-Miocene lava flows have been uplifted during the "fast rifting" in the Baikal area in the last 3–4 Ma and occur in the watershed areas of the Hamar-Daban range as "summit" lava covers and their relics in topographic highs (Kiselev et al. 1979; Logatchev and Zorin 1987). The Pliocene-Pleistocene basalts often form 'valley' lava flows in modern ravines and river valleys.

The 20 xenoliths used in this study are listed in Table 1. They have been collected at five sites in the western Hamar-Daban Range, including two occurrences in Pliocene-Pleistocene "valley" lava flows on its northwestern slope, two "summit" Miocene-Pliocene volcanic centres and a lava outcrop near Lake Baikal (Fig. 1). The Tumusun and Margasan volcanic centres are basaltic necks or dyke-like bodies that form summits in the watershed area topping a series of Miocene lave flows with a total thickness of about 500 m. Basaltic tuffs that appear to be associated with these eruption centres cover eroded Miocene basalts indicating late Miocene-Pliocene eruption ages. The xenoliths for this study were collected from the summit volcanic rocks whose K−Ar age is 5–7 Ma (Ashchepkov 1991). A sample of host basal 73-16b from the Tumusun volcano was cut from the lava fragment that entrained peridotite xenolith 73-16. One sample comes from a basaltic outcrop in the Suhaya river valley 15 km south of the town of Slyudyanka in northern Hamar-Daban (Fig. 1). The age of the host basalt is 18 Ma (unpublished K−Ar data of I. Ashchepkov)

Xenoliths in the young 'valley' basalts were collected in lava flows at two sites on the left bank of the Margasan river 20 km south of village Zun-Murino (Fig. 1). Most samples are from a lava flow with an age of 1 Ma; a nearby 4 Ma lava flow (unpublished K-Ar data of I. Ashchepkov) contains abundant cpx megacrysts, but very few xenoliths. A few other occurrences of mantle xenoliths are known in western Hamar-Daban that are not represented in our collection: Hubutuy river valley south of the Tumusun volcano and Mount Urunduchi (35 Ma) in western Hangarul ridge. Xenoliths from Bartoy locality in southern Hamar-Daban were described earlier (Ashchepkov 1991; Ionov et al. 1992b).

Sample preparation and analytical methods

Fresh material for bulk rock analyses and mineral separation was taken from central parts of the xenoliths taking care to avoid basaltic veins and altered material. The rocks were crushed by hand in a steel mortar and their aliquots ground in agate ball mills. Clinopyroxene (cpx) was separated magnetically from the 0.3–0.5 mm size fraction, then grains free of visible inclusions, cracks and surface contamination were hand-picked under microscope. The final cpx separates were leached in diluted HF and HCl and washed in distilled water and analysed by instrumental neutron activation analysis (INAA) or dissolved (without grinding) in a mixture of concentrated HF and $HClO_4$ for inductively coupled plasma (ICP-MS) or thermal ionisation (TIMS) mass-spectrometric analysis.

Major elements in bulk rocks were determined by X-ray fluorescence spectrometry (XRF) using glass fusion discs at Macquarie University. Na and K contents were obtained by flame photometry at Macquarie University and at Göttingen University (Ionov et al. 1992a). Mineral major element compositions were obtained on a Cameca Camebax JX 50 electron microprobe at Macquarie University using the WDS technique. The microprobe was used with 15 kV accelerating voltage, sample current of 10 nA and a beam diameter of 2–3 μm. Standards were natural and synthetic minerals, matrix corrections were done by PAP (Pouchou and Pichoir 1984) procedures.

Trace element analyses of five bulk rocks and two clinopyroxene separates were performed by ICP-MS on a VG PlasmaQuad instrument at Centre Géologique et Géophysique, Montpellier, following the procedure reported by Ionov et al. (1992c). Detection limits in the solids (taking into account chemical blanks) were 0.5–2 ppb for most REE, Rb, Nb, Ta, Hf, Th, U and 5–30 ppb for Sm, Zr, Sr, Ba, Pb and Sc. Precision was controlled by measurement of standard samples in each run and normally stayed within ±5% for element concentrations well above the detection limits. Two cpx separates were analysed by INAA using Ge(Li) detectors for γ-rays higher than about 100 KeV and an intrinsic Ge detector for energies below 150 KeV at the University of Cologne (courtesy of H.-G. Stosch). Clinopyroxene and feldspar were analysed using the proton-induced X-ray emission (PIXE) technique (Ryan et al. 1990) at CSIRO, Sydney. Clinopyroxene was analysed in grain mounts, feldspar (and some additional cpx grains) was analysed in situ in thin sections. Sr and Nd isotope analyses of a host basalt and four clinopyroxene separates were performed at the Cosmochemistry Division of Max-Planck-Institut für Chemie in Mainz, Germany using established procedures (Jagoutz and Wänke 1986).

Table 1 Summary of petrography, temperature estimates and mineral compositions for xenoliths (- absent. Abundance of spongy cpx shown as visual estimates relative to total cpx: *rare* ≤5%, *common* 5–30%, *abundant* 30–99%)

Locality Sample N°	Petrography			Temperature estimates (°C)			Mineral chemistry		
	Accessory feldspar	Spongy cpx	Foliation	Wells (1977) core-rim	Ca-opx[a] core-rim	opx-spl[a] core-rim	mg# in ol	Cr_2O_3 in spl	Al_2O_3 in cpx
Central Hamar-Daban, the Margasan volcano:									
83–36	common	rare	–	1005	1005–20	1015–50	0.893	8.6	7.0
83–50	rare	v. rare	weak	990–1015	1005–20	1020–45	0.895	8.4	6.8
83–69	common	rare	common	960–1000	990	980–995	0.897	10.5	6.5
T–1–30	–	rare	weak	975–1010	970–1030	990–1040	0.892	8.4	6.7
Central Hamar-Daban, the Tumusun volcano:									
XD–1	abundant	common	common	950–975	975–985	970	0.896	11.8	6.4
98–13	common	common	common	950	950	950–975	0.893	9.3	6.5
73–16	–	abundant	common	980–1005	970–990	990–1005	0.889	7.7	7.0
502–7	–	common	weak	995–1025	1010–30	1010–45	0.897	10.6	6.7
502–13	–	abundant	weak	955–985	970–995	990–1020	0.889	8.4	6.7
502–15	–	rare	–	1000–20	1005–25	1000–45	0.898	10.9	6.7
520–9	common	abundant	–	995	1005	980	0.901	16.2	5.9
Northwestern Hamar-Daban, lava flows in the Margasan river valley:									
AM–1	abundant	common	–	880	875–890	955–925	0.898	7.9	7.1
601–1	rare veins	–	common	965–1015	985–1030	940–975	0.908	26.1	4.5
601–3	rare	rare	common	975–1020	965–1020	970–1020	0.899	11.9	6.7
601–13	–	common	weak	1005–25	990–1025	995–1050	0.893	9.6	6.6
604–1	–	common	weak	1010–15	995–1015	1010–35	0.891	8.9	6.8
604–5	–	abundant	weak	980–1020	1005–1025	1035–60	0.878	6.9	7.2
604–7	–	–	strong	965–990	955–995	970–1005	0.898	13.1	5.9
604–15[b]	–	rare	–	980–1000	995–1015	1030	0.897	11.8	6.6
Northern Hamar-Daban, a lava flow south of Slyudyanka:									
SL–52[c]	–	common	weak	1145–1100	1125–15	1120–35	0.899	12.1	6.7

[a] Thermometers: *Ca-opx* Brey and Köhler (1990), *opx-spl* Sachtleben and Seck (1981); temperatures calculated at 15 kbar
[b] Contains accessory apatite
[c] Cores of largest pyroxenes yield the following *T* estimates: Wells 1093° C, Ca-opx 1070° C, opx-spl 1094° C

Rock microstructures and modal compositions

All xenoliths studied are spinel lherzolites. They have similar microstructures and grain size in all occurrences except Slyudyanka. Most common are foliated fine-grained lherzolites, less abundant are medium-grained protogranular rocks. Grain size in the foliated lherzolites is typically 1–2 mm for olivine (ol) and orthopyroxene (opx) and 0.5–1.0 mm for clinopyroxene and spinel (spl) but is significantly larger in the protogranular rocks: 2–4 mm for ol and opx and up to 1–2 mm for cpx and spl. Foliation in the rocks is defined by elongated pyroxenes and olivines and chain-like clusters of spinel. The degree of foliation varies strongly, and transitions between the fine-grained foliated and medium-grained protogranular microstructures are also present (Table 1). Strain features are not observed, and cores of pyroxenes usually have no exsolution lamellae.

Clinopyroxene-rich (12–16% cpx) lherzolites are the most common, with rare cpx-poor varieties. Many clinopyroxene grains are rimmed with fine-grained, spongy aggregates of secondary cpx (optically continuous with the parent grain) containing an intricate network of vermicular microchannels and rare feldspar inclusions. The spongy clinopyroxene is present in all samples studied except 604-7 (Table 1). The amount of the spongy cpx is quite variable within each sample but normally does not exceed 10% of the total cpx content (Table 1). However, in some samples much or all of the clinopyroxene has transformed into the spongy aggregate. No other minerals in the rocks appear to be affected by this process, and spinel grains inside or adjacent to the spongy cpx show no alteration (Fig. 2A).

Many rocks contain accessory feldspar (Table 1). Most commonly the feldspar occurs in fine-grained material adjacent to partially resorbed spinel and orthopyroxene. The fine-grained material commonly is made up of subhedral olivine (Fig. 2B) and feldspar, but may also contain clinopyroxene and very small grains of Cr-rich spinel or Ti-rich oxides (ilmenite or rutile, Fig. 2C). The feldspar typically occurs as interstitial material between the secondary olivine (Fig. 2B), but also forms larger aggregates made up of interlocking equant or prismatic grains (Figs. 2C, D). Both spinel and orthopyroxene grains in contact with such pockets are embayed and partially replaced by the feldspar-bearing fine-grained material (Fig. 2B), which may enclose relics of orthopyroxene optically continuous with a nearby opx grain. Many opx grains in sample 520-9 have been transformed into aggregates of fine-grained olivine with minor interstitial feldspar. The transparent brown or reddish spinel grains have spongy reaction rims consisting of black Cr-rich spinel and feldspar (Figs. 2B, C).

Less common are thin interstitial and cross-cutting feldspar veins. The veins are often connected with the fine-grained feldspar-bearing pockets around spinel and orthopyroxene (Fig. 2D). The distribution of the feldspar-bearing aggregates and veins is heterogeneous within a single hand-specimen so that one part of a xenolith or even of a single thin section may be relatively rich in these components and another entirely free of them. Both the textural position of the feldspar and its irregular distribution indicate textural disequilibrium. The feldspar veins and pockets in the xenoliths are sharply terminated at contacts with host basalt and show signs of thermal reaction. The host basalts consist of dark silicate glass with microlites of pyroxenes, feldspar and olivine; they are very different from the feldspar-bearing material in the

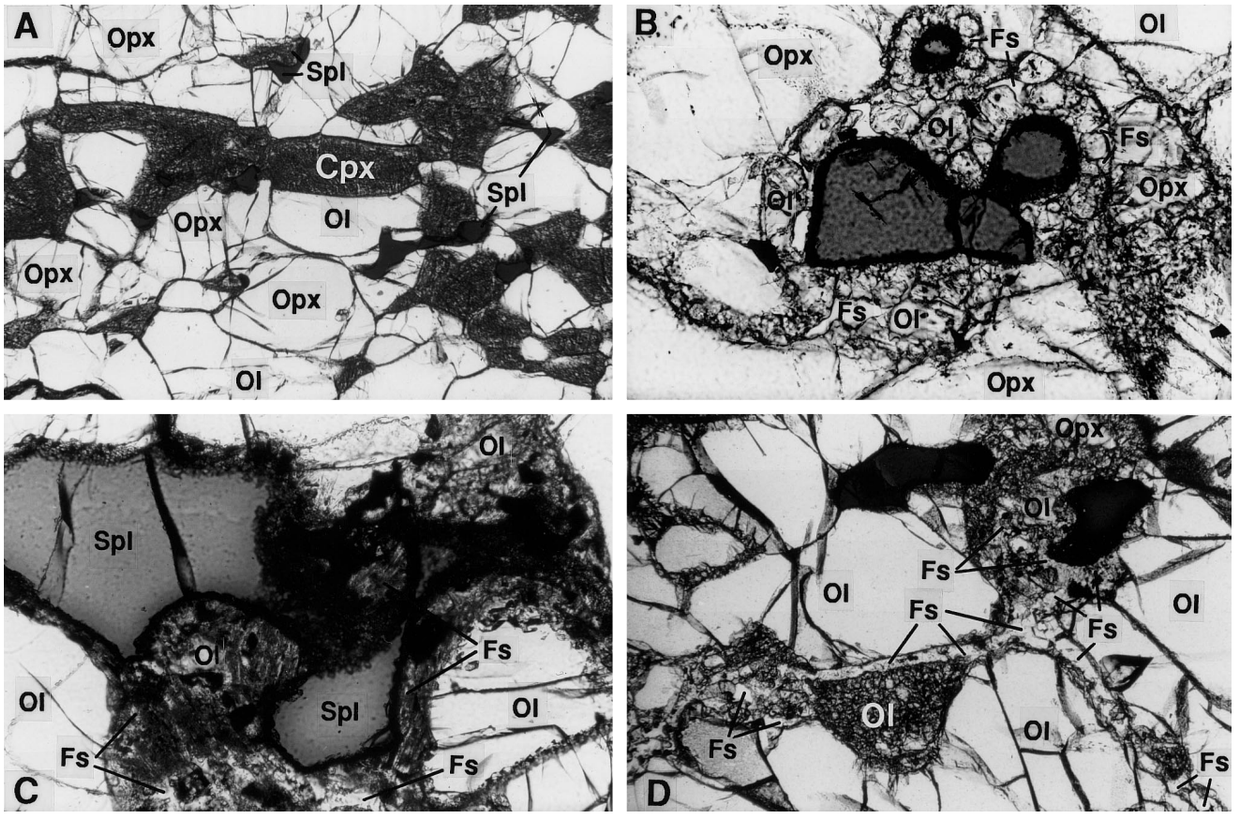

Fig. 2A–D Photomicrographs of Hamar-Daban xenoliths in plane-polarised transmitted light. **A** Spongy clinopyroxene (*Cpx*) in sample 604-5 completely replacing primary cpx. Spinel (*Spl*) and orthopyroxene (*Opx*) grains adjacent to cpx are not altered. In most other xenoliths spongy cpx occurs as rims around primary cpx and does not exceed 10–20% of the total cpx content. Field of view 5 mm. **B** Fine-grained olivine-feldspar aggregate replacing corroded spinel and orthopyroxene grains. The spinel is rimmed with a spongy aggregate of black chromite and alkali feldspar. Interstitial feldspar (*Fs*) occurs between subhedral olivine (*Ol*) grains. Sample 520-9, field of view 1.2 mm. **C** Same as (**B**), feldspar largely occurs as subhedral prismatic grains accompanied by tiny grains of Ti-rich oxides (which give to feldspar aggregates cloudy appearance) and Na, Al-poor cpx. Sample 98-13, field of view 1.2 mm. **D** Feldspar veins at grain boundaries of primary lherzolite minerals connected to a fine-grained olivine-feldspar pocket (*top right*) containinig resorbed spinel (*black*) and orthopyroxene. Sample XD-1, field of view 1.2 mm

xenoliths in colour, mineral assemblages and chemical composition and in particular the feldspar aggregates do not contain silicate glass. There are no textural or chemical indications that feldspar-bearing pockets and veins in the xenoliths are related to the host volcanic rocks.

Accessory sulphides are present in most rocks either as small interstitial grains or inclusions in silicate minerals (Ionov et al. 1992a). Sample 604-15 contains accessory apatite as small anhedral interstitial grains that have a turbid or vesicular appearance due to abundant fluid inclusions. No amphibole or phlogopite has been found in any of the samples in this study. Sample 83-69 contains a needle-shaped fine-grained aggregate of Na−K feldspar and rutile that may have been formed after a grain of amphibole or mica. Available Russian publications do not report any amphibole- or mica-bearing xenoliths from these and nearby localities (Kiselev et al. 1979; Ashchepkov 1991). However, rare peridotites with accessory phlogopite were reportedly found in the Margasan river valley by I. Ashchepkov. Pyroxenites (discrete xenoliths and veins in peridotites) occur in the Tumusun and Margasan volcanic centres, some containing kelyphitised garnet (Ashchepkov 1991).

Major element compositions and equalibration temperatures

Xenoliths from the Tumusun and Margasan volcanic centres commonly have moderately high contents of the "basaltic" major oxides: Al_2O_3, CaO, TiO_2, Na_2O. Their Mg numbers [mg# = $Mg/(Mg+Fe)_{at}$] range from 0.895 to 0.902 (Table 2); some xenoliths from the Margasan river valley are moderately depleted. The contents of CaO (Fig. 3), Al_2O_3, TiO_2 are negatively correlated with the MgO contents and Mg numbers as is common worldwide. Most of the Hamar-Daban xenoliths analysed plot on major element variation diagrams (Fig. 3A) in the middle of the compositional fields for common peridotites from other xenolith occurrences in the Baikal rift zone and northern Mongolia: Vitim, Bartoy and Tariat (Ionov 1986; Press et al. 1986; Ionov et al. 1992b, 1993).

A striking difference, however, is consistently high contents of K_2O (0.03 to 0.08%) and of Na_2O (Fig. 3B), in the Hamar-Daban peridotites (Table 2, Na and K analyses were obtained in two different laboratories). All

Table 2 Whole rock major element contents in selected xenoliths and a host basalt from Hamar-Daban (wt%, *blank entry* not determined)

	73-16b (Basalt)	73-16	83-36	83-50	83-69	98-13	XD-1	AM-1	520-9
SiO_2	46.85	45.72	45.46	44.85	44.69	44.80	44.98	45.02	44.02
TiO_2	2.00	0.16	0.153	0.134	0.114	0.134	0.13	0.12	0.05
Al_2O_3	14.56	3.91	4.12	3.57	3.14	3.58	3.14	3.89	2.26
Cr_2O_3		0.39	0.43	0.45	0.45	0.43	0.50	0.43	0.51
ΣFeO	10.30	8.13	8.12	8.06	8.02	8.08	7.97	7.91	8.23
MnO	0.16	0.12	0.13	0.13	0.13	0.13	0.14	0.14	0.11
MgO	10.29	38.29	39.01	40.06	41.27	40.06	39.68	39.83	43.45
NiO		0.25	0.25	0.25	0.26	0.25	0.27	0.25	0.29
CaO	8.89	3.52	3.32	3.10	2.54	2.99	3.26	3.22	1.50
Na_2O[a]	3.60	0.43	0.37	0.35	0.28	0.39	0.45	0.39	0.28
K_2O[a]	1.85	0.09[c]	0.033	0.053	0.045	0.082	0.10[c]	0.03[c]	0.10[c]
P_2O_5	0.58	0.00	0.00	0.00	0.00	0.00	0.00	0.00	0.00
Total	99.08	101.01	101.39	101.00	100.95	100.92	100.62	101.23	100.80
mg#	0.640	0.894	0.895	0.899	0.902	0.898	0.899	0.900	0.904
Ba (ppm)	467		2.2	1.5	1.5	2.0			
Sr (ppm)[b]	785	14[c]	13.5	13	9.5	12	17[c]	11[c]	7[c]

[a] Na and K determined by flame spectrometry
[b] Ba and Sr determined by ICP-AES at Göttingen University (Ionov et al. 1992a)
[c] K and Sr contents obtained by XRF at Macquarie University

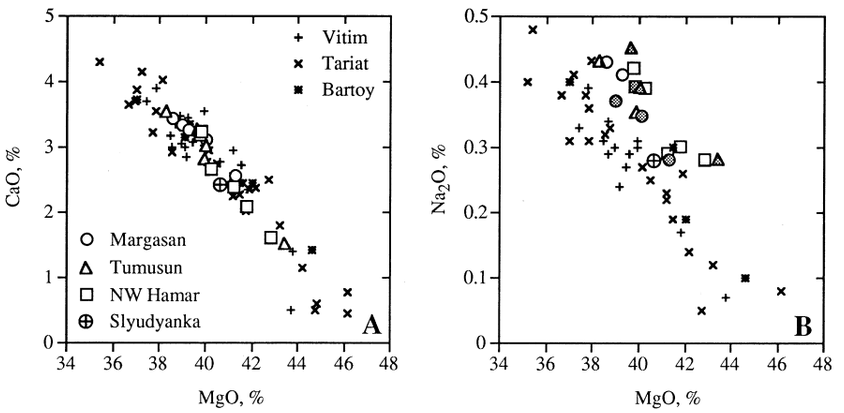

Fig. 3A Correlation between the contents of MgO and CaO and **B** between MgO and Na_2O (determined by flame photometry, this work and Ionov et al. 1992a) in peridotite xenoliths from Hamar-Daban in comparison with those from other localities south and east of Lake Baikal (Press et al. 1986; Ionov et al. 1992b; Ionov et al. 1993). Feldspar-bearing Hamar-Daban lherzolites are shown as *filled symbols* in plot **B**. The Hamar-Daban samples plot with other fertile peridotites in the MgO−CaO diagram, but above the MgO−Na_2O trend defined by the other xenolith suites because of their elevated Na_2O contents

peridotites from Tumusun and Margasan volcanic centres and Margasan river valley (both feldspar-bearing and feldspar-free) plot above the MgO−Na_2O trend defined by xenoliths from other sites in the BRZ (Fig. 3B) because of their elevated Na contents. The high K contents cannot be due to contamination or analytical errors as the Hamar-Daban samples were prepared (e.g. xenolith rims cut off) and analysed in the same manner as, and often together with, other xenoliths from Siberia and Mongolia that yielded low (≤0.01%) K contents (except some hydrous peridotites) (Ionov et al. 1992a). The high bulk rock Na and K contents possibly could be related to the presence of feldspar and spongy clinopyroxene.

Microprobe analyses of selected xenoliths are given in Table 3 and some additional information (mg# in ol, Cr_2O_3 in spl, Al_2O_3 in cpx) is provided in Table 1 for all samples studied. In all xenoliths except two the olivine Mg numbers are below 0.900, Cr_2O_3 contents in spinel are quite low (7 to 13%) and alumina contents in pyroxenes are high (6–7% in cpx). Overall, the mineral chemistry, in addition to the bulk rock major element compositions suggests the moderately fertile character of the mantle beneath Hamar-Daban.

Feldspar is compositionally variable, with CaO contents ranging from 0.05 to 10.8%, Na_2O from 3.9 to 8.1% and K_2O from 0.3 to 11.2% (Table 3); alkali-rich compositions are most common (Fig. 4). Feldspar grains of differing chemical compositions may be found nearby within a thin section. There is no general relationship between the textural position of feldspar (i.e. vein vs interstitial) and its composition. Feldspar is relatively rich in

Table 3 Representative electron microprobe analyses (wt%) of minerals [a] (*blank entries* below detection limit of 0.01–0.03%)

	XD-1						520-9						83-36				
	Opx	Cpx	Cpx	Spl	Feldspar		Opx	Cpx	Spl	Olivine		Fs	Opx	Cpx	Spl	Feldspar	
	Av. of 3	Av. of 4	Spongy	Av of 2			Av. of 5	Av. of 2	Av. of 3	Coarse	Fine-gr.		Av. of 5	Av. of 3			
SiO_2	54.90	51.79	50.70	0.05	62.28	63.55	55.45	52.43	0.06	40.74	66.79	54.57	51.45	0.07	54.34	65.24	
TiO_2	0.13	0.62	0.78	0.16	0.25	0.29	0.10	0.37	0.16			0.15	0.15	0.62	0.18	0.25	0.21
Al_2O_3	4.02	6.39	4.51	53.90	20.93	20.23	4.05	5.74	50.55			17.70	4.67	6.97	58.60	27.28	18.24
Cr_2O_3	0.35	0.84	0.89	11.80		0.06	0.45	1.05	16.20		0.08		0.29	0.69	8.57		
FeO	6.40	2.84	2.73	10.91	0.18	0.19	5.99	2.76	10.34	9.63	9.54	0.24	6.42	2.94	10.96	0.19	0.09
MnO	0.14	0.12	0.06			0.15	0.09		0.11	0.20	0.09	0.13	0.07		0.02		
MgO	32.60	14.75	16.51	20.45		0.05	32.94	15.51	20.11	48.99	49.25		31.75	14.75	21.66		
CaO	0.72	19.65	22.08		4.03	2.59	0.82	19.94		0.10	0.11	0.05	0.82	19.06		10.45	0.24
Na_3O	0.10	1.89	0.46		8.14	7.12	0.12	1.52				5.80	0.14	1.79		5.41	4.08
K_2O					1.83	4.37					8.62				0.27	11.10	
Total	99.35	98.88	98.72	97.26	97.64	98.45	100.07	99.41	97.40	99.57	99.92	99.44	98.94	98.34	100.04	98.21	99.20
mg#	0.901	0.902	0.915	0.770			0.907	0.909	0.776	0.901	0.902		0.898	0.899	0.779		

	83-69						98-13						83-50				
	Opx	Cpx	Spl core	Spl rim	Feldspar		Opx	Cpx	Cpx	Rutile	Feldspar		Opx	Cpx	Spl	Feldspar	
	Av. of 6	Av. of 4	Av. of 2	At fs			Av of 2	Av. of 3	In fs	In fs			Av of 2	Av. of 4			
SiO_2	55.03	51.98	0.08	0.09	56.19	65.60	55.43	51.98	53.41	0.15	55.85	63.89	54.48	51.68	0.06	61.12	65.58
TiO_2	0.14	0.60	0.16	0.79	0.31	0.24	0.12	0.65	1.77	94.93	0.20	0.23	0.14	0.61	0.18	0.35	0.10
Al_2O_3	4.39	6.49	56.45	47.44	26.43	18.35	4.06	6.54	1.54		26.14	20.22	4.62	6.80	57.82	23.10	19.38
Cr_2O_3	0.37	0.80	10.51	19.09	0.11	0.04	0.27	0.77	0.12	0.96			0.29	0.67	8.42		
FeO	6.26	2.70	9.28	10.74	0.20	0.13	6.48	2.83	3.14	0.29	0.22	0.19	6.16	2.92	11.99	0.31	0.13
MnO	0.12	0.08					0.17	0.10	0.09			0.03	0.13	0.11			0.02
MgO	32.69	14.89	20.47	19.09			32.59	14.59	18.43				32.00	14.77	21.52		
CaO	0.76	19.86			9.39	0.19	0.65	19.78	20.67	0.33	9.65	2.56	0.81	19.29		5.69	1.10
Na_2O	0.10	1.70			5.78	3.89	0.11	1.82	0.45		5.93	6.73	0.10	1.80		7.68	6.90
K_2O					0.56	11.20					0.40	5.39				1.00	6.34
Total	99.85	99.09	96.93	97.24	98.97	99.64	99.87	99.06	99.62	96.66	98.39	99.24	98.73	98.65		99.25	99.55
mg#	0.903	0.908	0.797	0.760			0.900	0.902	0.913				0.903	0.900	0.762		

[a] Core analyses are given for pyroxenes and spinel unless indicated otherwise

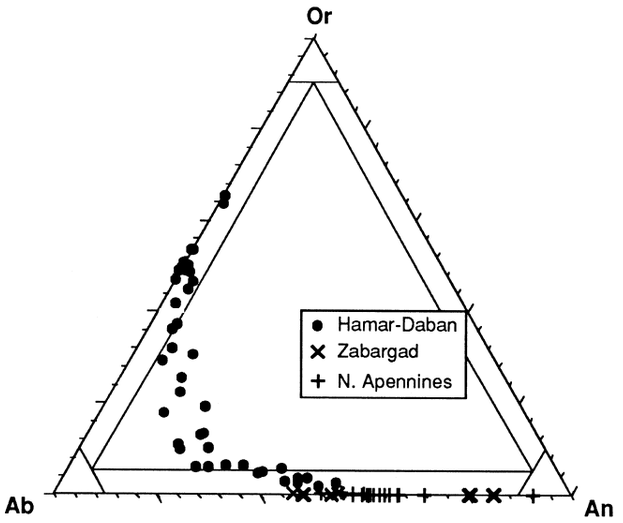

Fig. 4 Feldspar compositions in Hamar-Daban xenoliths and in peridotites from orogenic massifs in northern Appennines, Italy (Beccaluva et al. 1984; Rampone et al. 1995) and Zabargad Island (Bonatti et al. 1986; Piccardo et al. 1988). Feldspars in Hamar-Daban xenoliths have high content of orthoclase (*Or*) and albite (*Ab*), and low anorthite (*An*) content

titanium (0.15–0.35% TiO_2). Olivines show no zoning, and the fine-grained olivine grains replacing orthopyroxene (Fig. 2B) are very similar in composition to coarse primary olivines, except for higher contents of Cr and Mn in the former (sample 520-9, Table 3). No significant zoning has been found in spinel cores, but black spongy rims of spinels in reaction zones (Figs. 2B, C) are high in Cr, Fe and Ti (see sample 83-69, Table 3). Fine-grained clinopyroxene in feldspar-bearing aggregates is poor in Na and Al (sample 98-13, Table 3). Spongy rims of clinopyroxene are also poor in Na_2O (below 1%) and Al_2O_3, but rich in CaO (>20.5%). No glass has been found in their interstices, but rare feldspar inclusions occur.

In the majority of xenoliths pyroxenes have higher contents of Al and Cr in rims as compared with cores, as well as high Ca in orthopyroxene rims and lower Ca in clinopyroxene rims. The zoning is usually restricted to ~100 μm of the rims, whereas the cores of pyroxenes in the fine-grained foliated peridotites are homogeneous. This zoning pattern may indicate a recent heating event, or alternatively, incomplete equilibration during feldspar formation. In contrast, some protogranular and weakly foliated peridotites show unmixing in cores of pyroxenes, and their large (~3–4 mm) orthopyroxene grains (that may be relics of the original rocks little affected by deformation) are lower in Ca and Al than the smaller opx grains and may have preserved a record of slow cooling in the past.

Equilibration temperatures were estimated for cores and rims of pyroxenes using the two-pyroxene thermometer of Wells (1977), the Ca-opx thermometer of Brey and Köhler (1990) and the opx-spl thermometer of Sachtleben and Seck (1981) (Table 1). The values obtained from all three methods are very similar, in particular those for the Wells and Ca-opx thermometers (within 25° C). The opx-spl thermometer shows more scatter for some samples, probably because it is very sensitive to possible opx-spl disequilibrium due to mineral zoning (Sachtleben and Seck 1981). The rims of pyroxenes yield somewhat higher (by 5–40° C) temperatures than their cores for most samples (Table 1).

Both Wells and Ca-opx thermometers yield equilibration temperatures ranging from 950 to 1010° C and a single value of 880° C for cores of pyroxenes (except for the Slyudyanka occurrence). The temperature range for the xenoliths that come from four different occurrences is rather narrow indicating a uniform thermal regime in the uppermost mantle beneath the northwestern Hamar-Daban. They are well within a normal temperature distribution for spinel peridotites from active continental regions (O'Reilly and Griffin 1985) and indicate a generally higher lithospheric heat flow than continental shield areas. Equilibration temperatures for feldspar-bearing peridotites are similar or slightly lower than for feldspar-free ones, consistent with an interpretation of a shallow(er) location for these samples. The temperature range for the northwestern Hamar-Daban is more restricted than those obtained earlier for two other localities south of Lake Baikal: Bartoy, 890–1095° C (Ionov et al. 1992b), and Tariat, 880–1100° C (Ionov 1986; Press et al. 1986).

An earlier reconnaissance electron microprobe study of nine other peridotite xenoliths from the Slyudyanka occurrence (Ashchepkov 1991) indicated temperatures of 1120–1200° C (after Wells 1977) for eight samples and a value of ~900° C for a single one. Our detailed electron microprobe work on sample SL-52 has found that the cores of large (≥2 mm) pyroxene grains yield lower temperature estimates (1070–1090° C) than cores of small pyroxenes (1120–1145° C). It appears that the source region of the Slyudyanka suite has experienced a major heating event on a time scale that has not allowed complete re-equilibration of the minerals in coarse-grained peridotites.

Trace element and radiogenic isotope compositions

The ICP-MS and INAA trace element data are given in Table 4; the proton microprobe data are given in Tables 5 and 6. Some samples have been analysed for the same elements by different methods. The ICP-MS values for Rb, Sr, Nd and Sm in basalt 73-16b and Sr in cpx are within ±2% of those determined by TIMS isotope dilution (Table 7); values for Sm and Nd in the cpx are within 2–7% of the TIMS values. The contents of Sr and Zr determined by proton microprobe (by spot analysis of grain cores) in cpx 83-36 and 98-13 are within ±5% of the values obtained by ICP-MS on handpicked cpx grains. Overall, the ICP-MS data that make up a larger part of our database for trace elements are in very good

Table 4 Trace element composition (ppm) of bulk peridotites, clinopyroxene separates and a host basalt

	Basalt	Bulk peridotites				Clinopyroxenes			
	73-16b	83-36	83-50	83-69	98-13	83-36	83-50[a]	83-69[a]	98-13
Sc	21.8	21.1	18.7	16.4	16.1	62.4	65.3	66.5	69.6
Rb	34.3	0.33	0.60	0.60	0.77	0.033			0.028
Sr	732	15.7	13.7	9.40	12.5	82.7			83.4
Zr	187	7.05	6.27	4.49	6.05	36.1			35.8
Nb	46.2	0.128	0.122	0.081	0.355	0.305			0.208
Ba	459	1.69	1.37	1.29	1.56	0.03			0.06
La	31.6	0.437	0.236	0.186	0.538	1.26	1.01	1.04	2.85
Ce	64.6	1.26	0.727	0.551	1.30	4.31	3.46	3.70	6.78
Pr	7.53	0.181	0.131	0.104	0.179	0.837			1.05
Nd	30.6	0.932	0.752	0.582	0.872	4.89	3.74	3.56	5.38
Sm	6.08	0.322	0.285	0.222	0.288	1.91	1.91	1.98	1.89
Eu	2.01	0.136	0.120	0.090	0.116	0.801	0.77	0.71	0.771
Gd	5.87	0.499	0.457	0.335	0.425	2.93			2.85
Tb	0.788	0.090	0.083	0.060	0.077	0.542	0.52	0.57	0.528
Dy	4.53	0.620	0.589	0.416	0.533	3.73			3.65
Ho	0.830	0.139	0.133	0.093	0.118	0.828			0.813
Er	2.13	0.413	0.404	0.279	0.355	2.33			2.32
Tm	0.293	0.062	0.060	0.043	0.053	0.339	0.40	0.31	0.337
Yb	1.85	0.405	0.394	0.281	0.349	2.09	2.34	2.00	2.07
Lu	0.278	0.067	0.065	0.048	0.057	0.328	0.33	0.30	0.326
Hf	4.18	0.201	0.188	0.141	0.181	1.27	1.05	1.03	1.27
Ta	2.53	0.007	0.007	0.005	0.019	0.027			0.028
Pb	6.34	0.149	0.085	0.165	0.232	0.076			0.659
Th	3.41	0.013	0.011	0.011	0.130	0.029	0.225		0.761
U	1.04	0.0094	0.013	0.014	0.066	0.0095			0.284
Zr*[b]	1.30	0.82	0.83	0.78	0.81	0.71			0.72
Hf/Sm	0.69	0.63	0.66	0.64	0.63	0.67			0.67
Th/U	3.3	1.4	0.8	0.7	2.0	3.1			2.7

[a] INAA analyses (courtesy of H. Stosch)
[b] Zr*=Zr/[(Sm+Eu)/2], mantle-normalised (Hofmann 1988)

agreement with the TIMS and PIXE data. The INAA values for Nd and Sm in cpx 83-50 and 83-69 are systematically lower (by 9-16%) than those obtained by TIMS. The contents of Sr and Ba determined in five bulk rock samples by ICP-AES (Table 2) are in satisfactory agreement with the ICP-MS determinations, though the ICP-MS technique is more precise at low Ba and Sr contents.

The REE distribution patterns in the four bulk rock samples of peridotites from Tumusun and Margasan volcanoes are almost parallel to each other from Sm to Lu (Fig. 5). The contens of these moderately compatible REE are positively correlated with the contents of Ca and Al and negatively correlated with the Mg numbers of the rocks. The HREE contents in sample 83-36 are similar to their estimates for the primitive mantle Hofmann's (1988). All bulk rocks and clinopyroxenes except 98-13 have slight to moderate depletion in light REE (LREE). Sample 98-13 has an almost flat, slightly U-shaped REE pattern both in bulk rock and clinopyroxene due to a minor LREE enrichment superimposed on moderate depletion in intermediate REE relative to HREE. Clinopyroxene 83-36 shows a much more pronounced depletion in LREE than the bulk rock suggesting the presence of LREE-enriched intergranular material.

Unlike the relatively simple REE patterns, the trace element distribution plots for the xenoliths (including highly incompatible elements) are quite complex

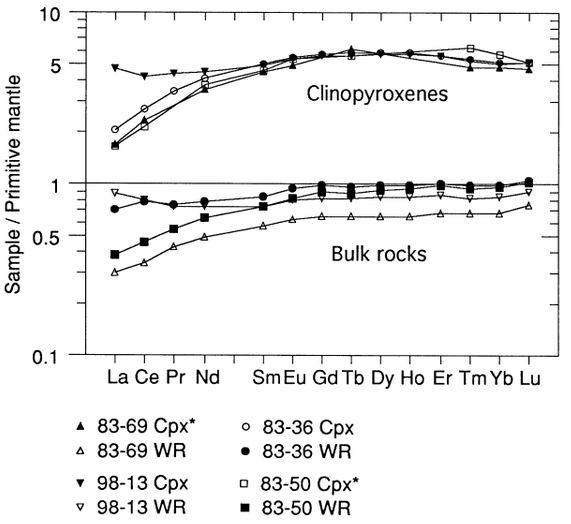

Fig. 5 Normalised (after Hofmann 1988) REE contents in bulk rock xenoliths and clinopyroxene separates. *INAA analyses

(Fig. 6B). Their most conspicuous features are marked positive anomalies for Rb, U, K and (in two samples only) Pb. The patterns for all the Hamar-Daban peridotites analysed have similar shapes suggesting that their anomalies may have similar origins for all the samples.

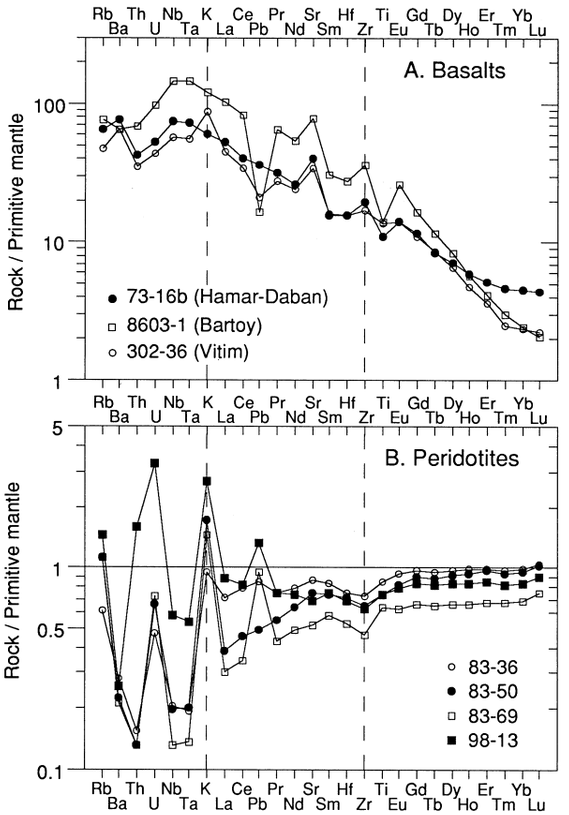

Fig. 6A, B Normalised abundance pattern diagrams. **A** Host basalt 73-16b from Hamar-Daban in comparison with representative basalts from the Bartoy and Vitim localities (Ionov and Hofmann 1995). **B** Bulk rock xenoliths from Hamar-Daban. All element abundances are normalised to their concentration in the primitive mantle (Hofmann 1988)

To interpret the patterns it is necessary, first of all, to distinguish between their mantle-derived components and possible contamination from host infiltration and posteruption alteration processes (Zindler and Jagoutz 1986).

Trace element distribution for the host basalt 73-16b from the Tumusun volcano (Fig. 6A) is very distinct from that the xenoliths. Contamination by host basalt therefore would be easy to identify. The very high contents of K and Rb in the Hamar-Daban xenoliths cannot be a result of infiltration of the host magma as the host basalts are rich in Nb and Ta and have high (Nb,Ta)/K,Rb) ratios, whereas the xenoliths have very low contents of Nb and Ta and low (Nb,Ta)/(K,Rb) ratios. Mass balance estimates based on data from Tables 2 and 4 indicate that the presence of as much as 1.8 to 4.5% and 1 to 2.2% of the basalt in the four xenoliths analysed would be required to explain their high contents of K and Rb respectively. However, even 1% contamination by the basalt would result in much higher bulk rock contents of Nb, Ta, Ba, Th than those measured (Table 4). Similar and other evidence has been used by Stosch et al. (1986), Zindler and Jagoutz (1986), and Ionov et al. (1992b) to conclude that host infiltration did not significantly affect the trace element composition of the bulk peridotite xenoliths from Mongolia, Arizona and Bartoy. Post-eruption alteration (e.g. by groundwater) can be a serious concern for elements that are known to be relatively mobile in sub-surface environments (U, Pb, K, Rb, Ba). In contrast to magma infiltration, its effects are difficult to define and identify. There is no petrographic evidence, however, for any significant post-eruption alteration in the xenoliths studied; they have no serpentine or smectite, although they may contain thin films of amorphous grain boundary material.

All four xenoliths shown in Fig. 6B contain accessory feldspar and it would be reasonable to suggest that the K and Rb in them reside in the feldspar (i.e. the rocks were enriched in K and Rb before their entrainment by basaltic magma). The contents of K and Rb in the feldspars are extremely variable; nevertheless rough estimates of their average contents can be made from the data in Tables 3 and 6: $\sim$5% for K_2O and 60 ppm for Rb. If these estimates are of the right order of magnitude, then the bulk rock contents of K and Rb would be consistent with the presence of about 1% of the feldspar, an estimate that does not contradict the petrographic observations. The contents of U and Pb in the feldspars are below detection limits of the proton probe, and we have no direct evidence to suggest that the U and Pb spikes in bulk peridotites could be attributed to the presence of feldspar.

Apart from the enrichment in alkalies and the U spike, the Margasan xenoliths 83-50 and 83-69 show consistent depletion in incompatible elements from intermediate and light REE to Nb, Ta and Th (Fig. 6B). Tumusun xenolith 98-13 has the highest contents of Th, U and Pb (as well as of K and Rb). Surprisingly, clinopyroxene is a major host for U, Th and Pb as well as of REE in the xenolith (Fig. 7A). The trace element pattern of the clinopyroxene is well correlated with that for the bulk rock (except that the cpx is very low in Nb, Ta, Rb and Ba), and the bulk rock enrichment in incompatible elements (except K and Rb) appears to reside largely in the clinopyroxene. In contrast, clinopyroxene 83-36 (Fig. 7B) shows consistent depletion in incompatible elements from LREE to Th and the cpx/bulk rock ratios are much lower for LREE than for HREE. It is not clear if feldspar may have contributed to the minor LREE enrichment in bulk 83-36 as the REE contents of feldspars are below detection limit of the proton probe (100–200 ppm). Overall, post-eruption alteration does not have to be invoked to explain the spikes in the trace element pattern of xenolith 98-13, as it can be adequately explained by the residence of K, Rb and Ba in accessory feldspar, and of Th, U and Pb in clinopyroxene. The bulk rock U spikes in the other three xenoliths result in very low Th/U ratios (Table 4) compared with the bulk earth value of 4 (3.1 in cpx 83-36) and might be due to post-eruption alteration.

All bulk rock xenoliths and clinopyroxenes have negative anomalies of high-field-strength elements (HFSE),

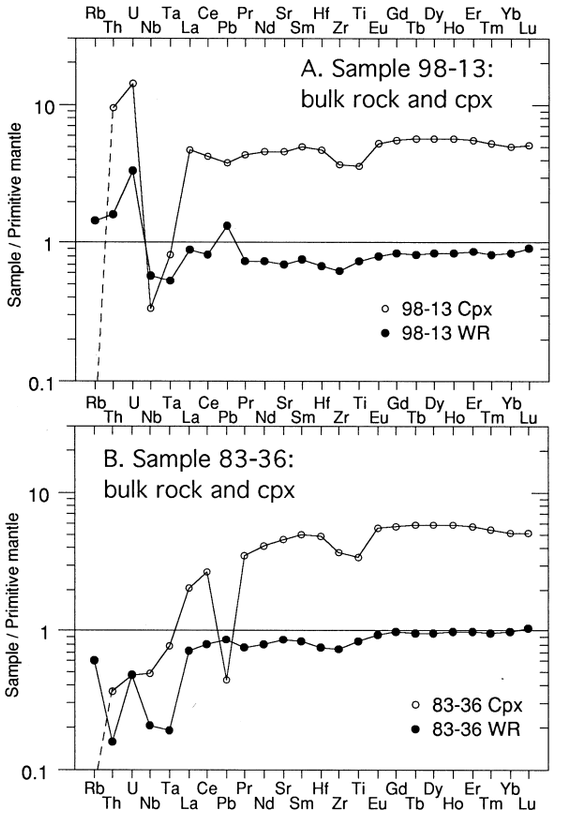

Fig. 7A, B Partitioning of trace elements between whole rock and clinopyroxene in two Hamar-Daban lherzolites from ICP-MS data (Table 4). All element abundances are normalised to their concentration in the primitive mantle (Hofmann 1988)

Table 5 Proton probe analyses of clinopyroxene (ppm)

Sample N°	Sr	Y	Zr	Ni	Zn
The Margasan volcano:					
83-36	83	19.1	38.0	393	16.3
83-50	82	19.6	36.6	376	14.3
83-69[a]	68	16.0	30.0	340	13.0
The Tumusun volcano:					
XD-1[a]	82	15.4	38.0	350	12.0
98-13[a]	79	18.8	37.7	333	9.2
73-16	77	18.3	33.6	338	14.4
502-7	78	14.4	29.3	380	12.0
502-13	70	18.0	31.7	338	14.5
502-15	75	15.1	29.9	344	14.3
520-9[a]	55	12.1	18.7	354	11.2
Lava flows, Margasan river valley:					
601-1	66	6.8	14.0	381	13.6
601-3	102	13.3	28.1	330	12.5
601-13	69	14.9	25.5	333	12.6
604-1	80	19.0	35.0	352	15.0
604-5	34-105	13–21	29–40	290–336	9 to 42
604-7	47	9.4	14.9	349	11.5

[a] Average of determinations in grain mounts and thin sections

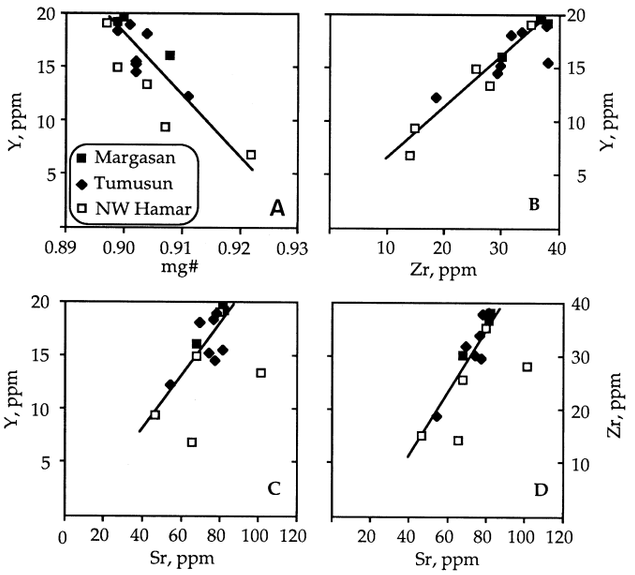

Fig. 8A–D Correlation between the contents of Sr, Zr and Y in clinopyroxenes from Hamar-Daban lherzolites obtained by proton microprobe, and the relation between their Mg number (mg#) and Y content (see text)

which have been defined as depletions or enrichments of the HFSE relative to the adjacent elements on compatibility diagrams (Figs. 6B, 7). In this paper we use the normalisation values and compatibility order after Hofmann (1988), which, in particular, defines the Zr anomaly as Zr*=Zr/[(Sm+Eu)/2]. Zr* in bulk rocks range from 0.78 to 0.83; two clinopyroxenes analysed have Zr* of 0.71 and 0.72 (Table 4). The negative Zr-Ti anomalies in bulk rocks are less pronounced than in clinopyroxene, which may be due to positive Ti and Zr anomalies in orthopyroxene (Rampone et al. 1991; McDonough et al. 1992). The Hf/Sm ratios in bulk rocks and clinopyroxenes are only marginally lower than the primitive mantle value of 0.69 (Table 4), and the negative anomalies are less pronounced for Hf than for Zr (Figs. 6B, 7).

Proton microprobe data for clinopyroxene and feldspar

Cores of large (>0.3 mm) clinopyroxene grains from 16 xenoliths were analysed by proton microprobe for Sr, Zr, Y, Ni, Zn (Table 5). These results refer to primary clinopyroxene only and to not document the composition of spongy clinopyroxene and of clinopyroxene possibly affected by feldspar formation (e.g. rims of primary grains adjacent to feldspar or fine-grained cpx in feldspar-bearing pockets). The contents of Sr, Zr and Y in the clinopyroxenes are negatively correlated with their Mg numbers (Fig. 8A) and the Cr/(Cr+Al) ratios of spinel. Clinopyroxenes in the 'fertile' xenoliths ($mg\#_{Ol}$=0.889-891, $Cr/(Cr+Al)_{Spl}$=6.9–8.5) contain 77–83 ppm Sr, 34–38 ppm Zr and 18–20 ppm Y as compared to ~55 ppm Sr, 15 ppm Zr and 7 ppm Y in the

moderately depleted xenoliths. Most xenoliths with low contents of Zr and Y in clinopyroxene are from NW Hamar-Daban (Fig. 8). There is a strong positive correlation between the contents of Zr and Y (Fig. 7B) and to a lesser extent for Zr−Sr and Y−Sr pairs (Figs. 7C, D). As a result, their elemental ratios are very similar in most samples: Sr/Zr=2.4±0.3, Sr/Y=4.5±0.4, and Zr/Y=1.9±0.2 (±2s). However, clinopyroxenes in xenoliths 601-1 and 601-3 (from NW Hamar-Daban) plot off the Zr−Sr and Y−Sr trends and have higher Sr/Zr and Sr/Y ratios because of relatively high contents of Sr (66 and 102 ppm respectively) at rather low contents of Zr (14 and 28 ppm) and Y (7 and 13 ppm). The high Sr may be due to metasomatic enrichment by a fluid rich in Sr, but poor in Y (HREE) and HFSE (e.g. O'Reilly et al. 1991; Ionov et al. 1994). The enrichment in Sr appears to be unrelated to feldspar formation as these two samples contain little feldspar, and only cores of clinopyroxene grains were analysed. The contents of all elements analysed are very variable in cpx 604-5, which is also less magnesian (mg#=0.88) than clinopyroxene in any other lherzolite. Sample 604-5, the two xenoliths with the Sr/Zr ratios in clinopyroxene that plot off the 'depletion' trend in Figs 8C and 8D, and the only xenolith with apatite, are from the young lava flows in the NW Hamar-Daban. Clinopyroxenes from this locality show more evidence for metasomatism than those from the Tumusun and Margasan volcanic centres.

Feldspar has extremely variable contents of Rb, Sr and Ba (Table 6): <2 to 149 ppm Rb, 40 to 3110 ppm Sr, 70 to 3590 ppm Ba. These great variations are observed both between feldspars from within a single thin section and different xenoliths. In sample 98-13, two small feldspar segregations adjacent to the same spinel grain have very different contents of Rb and Sr: 149 ppm Rb, 51 ppm Sr in one, and <2 ppm Rb, ~200 ppm Sr in the other; the K_2O contents in the same feldspar aggregates vary from 0.4 to 5.4%. With the small number of feldspar analyses done for each sample (three to five), it is not possible to conclude whether the data summarised in Table 6 may be typical for a given xenolith or are characteristic only of the specific feldspar grain or segregation analysed. The extreme variations of K, Rb, Sr, Ba in the feldspars indicate that they are not in equilibrium with each other within samples and are not in equilibrium with minerals of the host peridotite. Little data are available on trace element composition of feldspar in mantle peridotites. An ion probe study of plagioclase from lherzolites of the External Liguride units of the Northern Appennine orogenic belt in Italy (Rampone et al. 1993; Rampone et al. 1995) yielded a range of 70–170 ppm Sr and very low abundances of Y and Zr (<1 ppm); no Rb and Ba were reported and appear to be below the detection limit of ~1 ppm. The Hamar-Daban feldspars have markedly higher contents of Sr (and apparently of Rb and Ba) and may be related to an enrichment event.

Sr−Nd isotope compositions

Sr and Nd isotopic compositions of the four clinopyroxenes analysed plot within the "mantle array" (Fig. 9) in the upper-left part of the field of mid-ocean-ridge basalts (MORB), extending to higher than MORB $^{143}Nd/^{144}Nd$ and lower than MORB $^{87}Sr/^{86}Sr$ in the DMM field (Zindler and Hart 1986) and define a depleted mantle source region. The Hamar-Daban samples plot within the field outlined by LREE-depleted lherzolite xenoliths from three other central Asian localities: Vitim (Ionov and Jagoutz 1989), Bartoy (Ionov et al. 1992b), and Tariat (Stosch et al. 1986) (Fig. 9). The Sr−Nd isotopic compositions of the Hamar-Daban clinopyroxenes are very similar to those of unmetasomatised xenoliths from Bartoy and Tariat, and have somewhat lower $^{143}Nd/^{144}Nd$ at similar $^{87}Sr/^{86}Sr$ as compared with the majority of strongly depleted Vitim lherzolites. LREE-enriched cpx 98-13 plots in the low $^{143}Nd/^{144}Nd$-high $^{87}Sr/^{86}Sr$ end of this 'depleted' field, but distinctly away from the separate field defined by clinopyroxenes from metasomatised Bartoy and Tariat xenoliths that have much lower $^{143}Nd/^{144}Nd$ and higher $^{87}Sr/^{86}Sr$ values, suggesting distinct sources or/and timing of the metasomatic events.

The three LREE-depleted clinopyroxenes from the Margasan volcano (83-36, 83-50, 83-69) have very similar $^{147}Sm/^{144}Nd$ ratios of 0.243±0.04, and do not define an isochron that could constrain the age of depletion. However, their depletion age can be estimated if we as-

Table 6 Proton probe analyses of feldspar (ppm, *blank entries* below detection limit, high Ni values may be due to the presence of fine-grained olivine in feldspar segregations)

	Detect.	XD-1		520-9	83-69		98-13	
	limits	Av. vein	Pocket	Av. of 3	Av. of 2	Nº 5	Nº 12	Nº 13
Fe	20	900	2900	900	800	600	3500	9700
Ni	10	34	20		122	22	168	211
Cu	5	29	6		39	12	40	171
Zn	4		11		20	6	8	72
Ga	3	15	13	12	11	9	12	14
Rb	2	32	3	60	58	124	149	
Sr	4	1060	3110	860	143	41	49	206
Y	4							20
Ba	50	1555	2760	2520	195	70		
Rb/Sr		0.030	0.001	0.069	0.40	3.0	3.1	<0.01

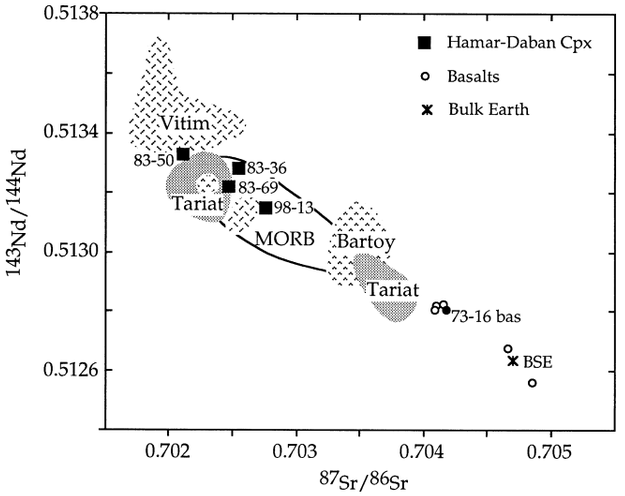

Fig. 9 Sr−Nd isotope composition of clinopyroxenes from Hamar-Daban xenoliths (*filled squares*) and of their host basalt (*filled circle*) (Ionov and Jagoutz, in preparation). Also shown are available data for other basalts from the Baikal region and central Mongolia (*empty circles*, Ionov et al. 1994), bulk silicate Earth (*BSE*) and fields for clinopyroxenes from the Vitim, Bartoy and Tariat occurrences (Stosch et al. 1986; Ionov and Jagoutz 1989; Ionov et al. 1992b)

sume that they were derived from a primitive mantle source and experienced only one depletion episode. Their Sm–Nd and Rb–Sr model ages calculated relative to bulk earth composition (Table 7) are fairly close to each other for each sample (within ±0.2 Ga) and therefore may be significant (Stosch et al. 1986). Altogether, the Sr and Nd model ages for the three clinopyroxenes define an age interval of 1.8 to 2.5 Ga, or even a narrower range of 1.8 to 2.1 Ga if the high Nd model age for 83-50 is discarded. The latter range is identical to that earlier obtained for LREE-depleted xenoliths from Tariat, Vitim, and Bartoy (Ionov et al. 1992b). The model age information indicates a major depletion event or a series of depletion episodes in the mantle beneath Hamar-Daban in the Proterozoic, probably about 2 Ga ago. The Rb−Sr model age of cpx 98-13 is quite high as well (1.6 Ga) and one can speculate than the rock also experienced a depletion event ~2 Ga ago followed by enrichment in LREE some time later. It appears that the LREE enrichment took place significantly later than the depletion event, as the Nd-isotope composition of the cpx 98-13 (with a low $^{147}Sm/^{144}Nd$ ratio of 0.20, which is close to the bulk earth value) has not evolved far from the depleted field defined by the LREE-depleted xenoliths (Fig. 9).

The host basalt 73-16b from the Tumusun volcano has a Sr−Nd isotopic composition very similar to those of basalts from two other localities in the Baikal region for which data are available [Bartoy (Housh et al. 1992; Ionov et al. 1992b) and Vitim (unpublished data of Ionov and Jagoutz 1991], but it is less radiogenic with respect to Sr and more radiogenic with respect to Nd than the host rocks for xenoliths from Tariat in central Mongolia (Stosch et al. 1986; Ionov et al. 1994) (Fig. 9). The very narrow range of Sr−Nd isotope compositions shown by the basalts from Hamar-Daban, Bartoy and Vitim suggests that late Cenozoic basalts in the Baikal region have been derived from an isotopically homogeneous mantle source region characterised by a moderate time-integrated depletion in incompatible elements relative to the bulk earth composition. On the other hand, the Tumusun basalt has higher contents of HREE and Sc, a higher Mg number (0.64) and lower alkali contents than xenolith-bearing basalts from Bartoy and Vitim (Ionov and Hofmann 1995).

Table 7 Concentrations of K, Rb, Sr, Sm and Nd and Sr−Nd isotope data (data after Ionov and Jagoutz (in preparation), *n.d.* not determined)

	Host basalt	Clinopyroxenes from peridotite xenoliths:			
	73-16b	83-36	83-50	83-69	98-13
Sample wt (mg)	66.0	11.8	6.3	13.4	19.3
K, ppm	13670	40.6	47.3	n.d.	n.d.
Rb, ppm	33.7	0.020	0.011	n.d.	n.d.
Sr, ppm	716.5	80.9	80.4	74.1	81.6
Sm, ppm	6.21	1.86	1.76	1.73	1.77
Nd, ppm	30.0	4.58	4.43	4.23	5.29
$^{147}Sm/^{144}Nd$	0.125	0.245	0.240	0.247	0.202
$^{143}Nd/^{144}Nd$[a]	0.51278±2	0.51325±4	0.51330±2	0.51319±2	0.51312±2
ε_{Nd}[b]	2.2	12.0	12.9	10.8	9.4
$^{87}Rb/^{86}Sr$	0.136	0.00073	0.00041	n.d.	n.d.
$^{87}Sr/^{86}Sr$	0.70419±2	0.70254±2	0.70211±2	0.70247±3	0.70276±2
Nd model age, Ga[c]		2.05	2.47	1.78	/13.5/
Sr model age, Ga[d]		1.77	2.11	1.81	1.57

[a] $^{143}Nd/^{144}Nd$ as measured
[b] ε_{Nd} adjusted by −0.6 (Jagoutz and Wänke 1986)
[c] Sm−Nd model ages calculated with $^{147}Sm/^{144}Nd=0.1966$, $^{143}Nd/^{144}Nd=0.512636$
[d] Rb−Sr ages calculated with $Rb/Sr=0.03$, and $^{87}Sr/^{86}Sr=0.7047$ (bulk earth)

The origin of feldspar in mantle peridotites

Experimental constraints

Experimental studies of reactions between the end members forsterite (Fo) and anorthite (An) (Kushiro and Yoder 1966) have shown that they are stable at less than 8.5 ± 0.5 kbar at 1250° C, but ol+opx+cpx+spl is the stable assemblage at higher pressures. The pressure of the transition between plagioclase and spinel stability fields in the system $CaO-MgO-Al_2O_3-SiO_2$ (CMAS) is temperature dependent and varies between about 6.5 kbar at 900° C and 9 kbar at 1300° C (Green and Hibberson 1970; Herzberg 1978). These results, however, cannot be directly applied to natural peridotites that contain appreciable amounts of Na and Cr, e.g. the presence of sodium enlarges the depth region over which plagioclase lherzolite can exist (Windom and Unger 1988). The phase transitions in the peridotites are controlled by coupled and sliding reactions involving changes in plagioclase and spinel solid solutions and thus occur over a range of pressures at a given temperature. A study of reactions between magnesian olivine (Fo_{92}) and labradorite (An_{59}), and between olivine and plagioclase in a complex pyrolite composition (Green and Hibberson 1970) has found that there is a 5-phase field of ol+opx+cpx+pl+Al−spl between 9 kbar and 11–14 kbar (depending on composition) at 1200° C in which plagioclase content in bulk rock decreases with increasing pressure. It should be noted that the high-*P*,*T* boundary for the stability field of plagioclase could not be very tightly located in the experiments, because of the difficulty of distinguishing small amounts of plagioclase from possible incipient melting (Green and Hibberson 1970). Pure albite (Ab) is stable in the Ab-Fo system up to about 18 kbar at 900° C and 23 kbar at 1225° C (Windom and Unger 1988); sanidine ($KAlSiO_4$) is stable in association with forsterite up to 20 kbar at 1000° C (Wendlandt and Eggler 1980). Thus the experimental data suggest that plagioclase may be stable in fertile peridotites up to 8–9 kbar at 800° C and 11–12 kbar at 1200° C (Green and Hibberson 1970; Jaques and Green 1980), whereas alkali feldspars can be stable at somewhat higher pressures.

Equilibration pressures for the feldspar-bearing Hamar-Daban xenoliths are not known, but they can be roughly estimated from the depth to Moho (referred to as crustal thicknesses by Zorin et al. 1989) obtained by regional seismic and gravity studies: ~45 km for the Hamar-Daban Range decreasing northwards to about 40 km at the southern shore of Lake Baikal. Assuming the average crustal density of ~2.8 g/cm^3 (Zorin et al. 1989), this suggests pressure may be about 12 kbar just below the crust/mantle boundary. This estimate is higher than the upper limit of 10–11 kbar of plagioclase stability inferred for fertile peridotites at ~1000° C (Creen and Hibberson 1970; Jaques and Green 1980). The composition of feldspars in the Hamar-Daban xenoliths is quite variable, but they are in general poor in Ca and rich in Na and K (Table 3). Such alkali-rich feldspars could possibly be stable in mantle peridotites at somewhat higher pressures than the K-poor plagioclase with moderate Na contents in the experimental work on model peridotites.

Possible effects of metasomatism

The common location of feldspar-bearing aggregates between adjacent spinel and orthopyroxene grains (Fig. 2B), the ubiquitous association of the feldspar with fine-grained olivine, and the available experimental data, indicate that the feldspars in the Hamar-Daban lherzolites were formed as a result of the reaction: Al−opx +Na−Al-cpx+Al−spl+K−Na-bearing fluid=ol+Na −K−Ca−fs+Cr−spl. For example, the reaction between olivine and labradorite was approximated by Green and Hibberson (1970) as follows:

$$\underset{\text{labradorite}}{3CaAl_2Si_2O_8 \cdot 2NaAlSi_3O_8} + \underset{\text{olivine}}{8Mg_2SiO_4}$$

$$= \underset{\text{omphacite}}{3CaMgSi_2O_6 \cdot 2NaAlSi2O_6} + \underset{\text{enstatite}}{10MgSiO3} + \underset{\text{spinel}}{3MgAl_2O_4}$$

The high K contents of the feldspars replacing spinel and pyroxene as well as the presence of K-rich feldspar veins necessitate addition of K to the peridotites as little potassium is present in the pyroxenes (≤50 ppm in the cpx, Table 7) and spinel in the xenoliths. The contents of K and Rb (to a lesser extent Na_2O, Fig. 3B) in bulk rock xenoliths from Hamar-Daban are high relative to common anhydrous peridotite xenoliths and even to some hydrous peridotites. For example, the average contents of K (435 ppm) and Rb (0.57 ppm) in the four Hamar-Daban xenoliths analysed are higher than for amphibole lherzolite xenoliths from the nearby Bartoy volcanoes (270 ppm K and 0.23 ppm Rb) (Ionov and Hofmann 1995). The experimental constraints and trace element evidence strongly suggest that the formation of feldspars in the mantle beneath Hamar-Daban was a result of a metasomatic event that enriched mantle rocks in potassium and other alkalies.

The nature of that event and of the media responsible for the metasomatism remain uncertain. Particularly surprising is that trace element patterns of the Hamar-Daban xenoliths (Fig. 6B) show marked K and Rb spikes, but no strong enrichment in other incompatible elements (except U). The available evidence appears to suggest that the enrichment was caused by an exotic fluid rich in K, Rb and Na (possibly U), rather than by a silicate melt. Melt compositions identical to the troctolitic (ol+fs) or feldspathic pockets and veins apparently cannot be produced by mantle igneous processes. Many feldspars are too rich in Rb (30–150 ppm, Table 6) to have precipitated from a basaltic melt (e.g. like 73-16b) considering that $D_{Rb}^{fs/melt}$ is well below unity both for plagioclase and alkali feldspars (Ewart and Griffin 1994). Mantle metasoma-

tism by a silicate melt would probably produce enrichment in other incompatible elements (e.g. Nb, Th, La) in addition to alkalies (an argument used earlier to rule out xenolith contamination by host magma). The absence of amphibole and mica in the Hamar-Daban xenolith suite apparently indicates 'dry' conditions in their source regions and suggests that the inferred metasomatising fluid was poor in water since it precipitated feldspar rather than the alkali-rich 'hydrous' minerals. By-products of the fluid-induced reaction consuming Ti-bearing pyroxenes and spinel to produce feldspar and olivine are tiny grains of Ti-rich oxides, rutile and ilmenite in the feldspar aggregates, and high titanium contents (0.15–0.40%) in the feldspars (in hydrous peridotites Ti is commonly accommodated by amphiboles and mica). The alkali-rich, water-poor fluid may probably consist largely of CO_2, though its origin remains to be established.

A genetic link between feldspar-rich veins in the xenoliths and host basaltic magma has been suggested previously (Ashchepkov 1991). However, this is not consistent with the new textural observations, trace element data and major element compositions of the vein minerals obtained in the present study.

Comparisons with other occurrences of feldspar peridotites

Mantle xenolith suites with feldspar-bearing peridotites are extremely rare, as the plagioclase peridotite stability field constrains their occurrence on the continents to areas with crust $<$40 km thick and high geothermal gradient. Limited occurrences have been reported mostly from regions of marked extension such as the Basin and Range province of the southwestern USA. Rare pl-bearing peridotite xenoliths have been found (together with more abundant pl-bearing websterites and composite peridotite-gabbro xenoliths) in the Cima volcanic field, California, where the present-day Moho is at $\sim$27–30 km (Wilshire et al. 1991). Plagioclase in the Cima peridotites occurs either as coronas around spinel or is texturally equilibrated with the peridotite; its composition ranges from An_{48} to An_{66} with Or contents of 0–1%. Wells (1977) equilibration temperatures of the plagioclase peridotites range from 960 to 1005° C. Plagioclase formation is attributed to infiltration of spinel peridotites by basaltic melts often followed by deformation and recrystallisation. Amphibole and phlogopite occur in many peridotite xenoliths including pl-bearing rocks (Wilshire et al. 1991).

Four plagioclase-bearing lherzolite xenoliths have been reported from Oahu, Hawaii (Sen 1988). All these rocks exhibit strong foliation and porphyroclastic texture whereas such strong deformation is not seen in other peridotite xenoliths from the same locality. Plagioclase crystals of equant habit occur in the groundmass, as well as tiny grains of zoned spinel with highly variable composition. Wells' (1977) thermometer yielded 960–1010° C for neoblast crystallisation. Rare accessory plagioclase (K-poor) was found in some peridotite xenoliths from eastern Sikhote-Alin near the Pacific coast of Siberia where the crust in thin (Ionov et al. 1995), and from north China and eastern Australia (H. Ma and O. Gaul, personal communications, 1995).

Plagioclase peridotites are common in orogenic peridotite massifs believed to be slices of the upper mantle tectonically emplaced into the crust, e.g. Ronda (Frey et al. 1985), Lanzo (Boudier 1978) and other massifs in northern Italy (Beccaluva et al. 1984; Rampone et al. 1995), and peridotites on the Island of Zabargad in the Red Sea (Bonatti et al. 1986). Two groups of plagioclase-bearing rocks are commonly identified based on the plagioclase content and textural position (Bonatti et al. 1986; Rampone et al. 1995). In spinel lherzolites with accessory ($<$2%) plagioclase, it is confined to thin rims around Al-rich spinels and fine-grained aggregates of pl+ol+px. Plagioclase lherzolites ($>$2% pl) are most common, they contain broad ($\sim$0.5–1.0 mm) rims of equigranular plagioclase around Cr-rich spinels, granoblastic ol+pl+px domains and pl exsolution within clinopyroxene. On Zabargad Island, the pl-peridotites have textures ranging from porphyroclastic to cataclastic, indicating various degrees of tectonic deformation. They are found in localised zones or bands (often together with amphibole peridotites) within protogranular spinel lherzolite that makes up largest part of the peridotite body; some rocks have pl-rich veins forming a network around elongated lherzolite lenses. Plagioclase composition (Fig. 4) in fertile lherzolites commonly ranges from An_{45} to An_{70}; some pl-peridotites have more calcic plagioclase, An_{80} to An_{93} (Bonatti et al. 1986; Piccardo et al. 1988; Rampone et al. 1993). The contents of K_2O in plagioclase from all orogenic massifs are very low and do not exceed 0.1% (including plagioclase from gabbroic rocks) (Boudier 1978; Beccaluva et al. 1984; Bonatti et al. 1986; Piccardo et al. 1988; Rampone et al. 1993). Spinels in pl-peridotites have higher Cr/(Cr+Al) ratios, and clinopyroxenes have lower Na and Al contents relative to spinel lherzolites. Pl-peridotites typically have equilibration temperatures of 850–950° C (Bonatti et al. 1986; Woodland et al. 1992; Rampone et al. 1995).

The origin of plagioclase in orogenic massifs is attributed to decompression during uplift and magmatic or metasomatic processes. Clinopyroxenes from pl-lherzolites in the External Liguride massifs or northern Italy were found to have much lower Sr contents than clinopyroxenes from spinel lherzolites (Rampone et al. 1993) and show decoupling in the behavior of Sr and Zr. Rampone (1993) attributed the trace element patterns to subsolidus re-equilibration of spinel lherzolites in a closed system and explained the origin of plagioclase by metamorphic evolution during decompression, without the occurrence of igneous processes. Bonatti et al. (1986) noted that the Zabargad pl-peridotites tend to be richer in Ca and Al relative to the spinel lherzolites, and attributed the origin of these plagioclase peridotites to crystallisation of a small fraction of 'exotic', extraneous basaltic

melts trapped in spinel peridotites with subsequent re-equilibration. Piccardo et al. (1988) explained plagioclase formation by incomplete metamorphic equilibration during decompression assisted by crystallisation of liquids, produced locally by an incipient low-pressure partial melting. Woodland et al. (1992) suggested that the presence of metasomatic fluids locally assisted plagioclase-forming reaction in Ronda rocks. Kurat et al. (1993) argued that plagioclase-rich veins in Zabargad peridotites were formed as a result of metasomatic, rather than igneous processes.

Plagioclase peridotites are locally abundant at a few oceanic localities, notably at St. Paul's Rocks, the ocean floor off the Galicia coast and the Romanche Fracture Zone, and some studies suggest that overall about 1/3 of abyssal peridotites appear to have once contained plagioclase (Dick and Bullen 1984). Spinels in abyssal pl-peridotites are richer in TiO_2 and Fe_2O_3 and tend to be more Cr-rich as compared to spinels in pl-free peridotites from the same localities. These features can be attributed to a reaction between Al-spinel and a melt to produce plagioclase and Cr-spinel, and abyssal pl-peridotites can be considered as hybrid rocks formed by crystallisation of trapped melt in a mantle tectonite (Dick and Bullen 1984).

Overall, there are some common features between feldspar-bearing xenoliths from Hamar-Daban and pl-peridotites reported from other localities worldwide, e.g. reaction relationships of feldspar with Al-spinel are widespread. A link between pl-rich peridotites and tectonic deformation has been documented both in alpine-type massifs (Zabargad, Lanzo) and xenolith suites from Cima, California and Oahu, Hawaii. Foliation is also common in the xenoliths from the four sites in Hamar-Daban.

However, some aspects of petrology and geochemistry of the feldspar-bearing peridotites from Hamar-Daban are unique for that xenolith suite: (1) the feldspar compositions are richer in Na, Ti and particularly K than in any other peridotite suite for which chemical data are available (Fig. 4), (2) many feldspars are very rich in Rb, Sr, and Ba, (3) feldspars are locally heterogeneous in terms of major and trace element compositions, they show strong textural and chemical disequilibrium with host peridotites and no evidence of re-equilibration,(4) reaction relationships of feldspar with orthopyroxene and the presence of spongy clinopyroxene are quite common, (5) no amphibole and mica have been found in the Hamar-Daban xenoliths, (6) there is no unequivocal textural or chemical evidence for trapped or injected silicate melt, though trace element data suggest enrichment in alkalies, and (7) crustal thickness beneath Hamar-Daban suggests a greater depth of origin than for other known series of feldspar peridotites. This evidence strongly suggests that the formation of feldspar in the Hamar-Daban mantle was a relatively recent event and that it was related to infiltration of an alkali-rich, H_2O-poor fluid into spinel peridotites. A distinctive feature of feldspars from the Hamar-Daban xenoliths appears to be a significant and commonly very high content of potassium, whereas plagioclase from orogenic lherzolites is typically very poor in K ($\leq$0.1% K_2O, Fig. 4).

The nature of the uppermost mantle beneath the Hamar-Daban

Peridotite xenoliths studied from the four sites (Tumusun and Margasan volcanoes and two lava flows in the Margasan river valley) have similar textures, modes, chemical compositions and equilibration temperatures. It can be concluded therefore that the mantle in northwestern Hamar-Daban has consistent characteristics for at least 50 km across (i.e. between the xenolith occurrences studied) at the depths sampled. Typical of this mantle domain is the fine grain size and foliation of the peridotites, fertile or moderately depleted modal and major element compositions, the absence (or extreme paucity) of amphibole and mica and the ubiquitous presence of intergranular feldspar and spongy clinopyroxene.

The textural, chemical and isotopic data indicate a complex history for this mantle domain. Most xenoliths studied show regular correlations between the contents of major elements and compatible trace elements in rocks and minerals (Figs. 3, 8); many lherzolites and their clinopyroxenes are depleted in LREE and other incompatible trace elements (Figs. 5, 6). These relationships appear to be consistent with the origin of the peridotite series as a result of variable degrees of extraction of partial melts from an originally homogeneous fertile lherzolite (Frey et al. 1985). The relatively high contents of Sr (Figs. 8C, D), LREE, Th and U (Fig. 7A) in some clinopyroxenes suggest subsequent local enrichment episode(s) that occurred well before the eruption of host basalts. Bulk rock enrichment in alkalies and formation of feldspar and spongy clinopyroxene was the latest and relatively recent event.

This young event may have been related to the development of the Baikal rift north and west of Hamar-Daban. Some workers relate the "fast rifting" in the last 3–4 Ma to an asthenospheric upwelling (Logatchev and Zorin 1987) that allegedly reached the base of the crust in the broad area southeast of Lake Baikal. However, our data do not indicate any significant differences between the younger Pleistocene-Pliocene (1–4 Ma) and the older (probably "pre-rift") Pliocene-Miocene (5–7 Ma) xenolith suites. Equilibration temperatures of the Hamar-Daban xenoliths are not higher than for those from other occurrences in the region located further from the rift and are well below temperatures expected for mantle diapirs (Logatchev and Zorin 1987). Therefore, the northwestern Hamar-Daban area appears to be beyond the zone (probably restricted to the rift axis) where the recent active rifting has significantly affected the lithospheric mantle. This study and other work on mantle xenoliths in the Baikal region (Ionov et al. 1992b; Kiselev and Popov 1992) found no evidence that the

"anomalous mantle" beneath the BRZ defined by low P-wave velocities immediately beneath the Moho (7.7–7.8 km/s) consists of partially melted rocks.

Acknowledgements We wish to thank S. Esin and U. Litasov for help with collecting samples, V.S. Antipin for providing two xenoliths for our study, C. Dupuy and L. Savoyant for support and assistance with ICP-MS analyses, W.L. Griffin and Tin Tin Win for assistance with proton microprobe analyses, E. Jagoutz for availability of the Sr−Nd isotope facilities, H.-G. Stosch for INAA data on two cpx separates and N. Pearson for help with electron microprobe analyses. The study was supported by a Macquarie University Research Fellowship and an ARC Fellowship to D.A. Ionov and ARC and Macquarie University research grants to S.Y. O'Reilly.

References

Ashchepkov IV (1991) Deep-seated xenoliths of the Baikal rift (in Russian). Nauka, Novosibirsk

Beccaluva L, Macciotta G, Piccardo GB, Zeda O (1984) Petrology of lherzolitic rocks from the Northern Apennine ophiolites. Lithos 17: 299–316

Bonatti E, Ottonello G, Hamlyn PR (1986) Peridotites from the island of Zabargad (St. John), Red Sea: petrology and geochemistry. J Geophys Res 91: 599–631

Boudier F (1978) Structure and petrology of the Lanzo peridotite massif (Piedmont Alps). Geol Soc Am Bull 89: 1574–1591

Brey GP, Köhler T (1990) Geothermobarometry in four-phase lherzolites II. New thermobarometers, and practical assessment of existing thermobarometers. J Petrol 31: 1353–1378

Dick HJB, Bullen T (1984) Chromian spinel as a petrogenetic indicator in abyssal and alpine-type peridotites and spatially associated lavas. Contrib Mineral Petrol 86: 54–76

Ewart A, Griffin WL (1994) Application of proton-microprobe data to trace element partitioning in volcanic rocks. Chem Geol 117: 251–284

Frey FA, Suen CJ, Stockman HW (1985) The Ronda high temperature peridotite: geochemistry and petrogenesis. Geochim Cosmochim Acta 49: 2469–2491

Green DH, Hibberson W (1970) The instability of plagioclase in peridotite at high pressure. Lithos 3: 209–221

Herzberg CT (1978) Pyroxene geothermometry and geobarometry: experimental and thermodynamic evaluation of some subsolidus phase relations involving pyroxenes in the system $CaO-MgO-Al_2O_3-SiO_2$. Geochim Cosmochim Acta 42: 945–957

Hofmann AW (1988) Chemical differentiation of the earth: the relationship between mantle, continental crust, and oceanic crust. Earth Planet Sci Lett 90: 297–314

Housh T, Bowring SA, Luhr JF, Rasskazov SV (1992) Isotopic constraints on the evolution of late Cenozoic magnatism in the southern Baikal rift (abstract). Eos Trans Am Geophys Union 73(14), Spring Meeting Suppl:333–334

Ionov DA (1986) Spinel peridotite xenoliths from the Shavaryn-Tsaram volcano, northern Mongolia: petrography, major element chemistry and mineralogy. Geol Zbornik – Geologica Carpathica 37: 681–692

Ionov DA, Hofmann AW (1995) Nb-Ta-rich mantle amphiboles and micas: implications for subduction-related metasomatic trace element fractionations. Earth Planet Sci Lett 131: 341–356

Ionov DA, Jagoutz E (1989) Sr and Nd isotopic composition in minerals of garnet and spinel peridotite xenoliths from the Vitim Highland: first data for mantle inclusions the USSR. Trans. (Doklady) USSR Acad Sci: Earth Sci Sect 301: 232–236

Ionov DA, Hoefs J, Wedepohl KH, Wiechert U (1992a) Content and isotopic composition of sulphur in ultramafic xenoliths from central Asia. Earth Planet Sci Lett 111: 269–286

Ionov DA, Ashchepkov IV, Stosch H-G, Witt-Eickschen G, Seck HA (1993) Garnet peridotite xenoliths from the Vitim volcanic field, Baikal region: the nature of the garnet-spinel peridotite transition zone in the continental mantle. J Petrol 34: 1141–1175

Ionov DA, Savoyant L, Dupuy C (1992c) Application of the ICP-MS technique to trace element analysis of peridotites and their minerals. Geostandards Newsletter 16: 311–315

Ionov DA, Prikhod'ko VS, O'Reilly SY (1995) Peridotite xenoliths from the Sikhote-Alin, south-eastern Siberia, Russia: trace element signatures of mantle beneath a convergent continental margin. Chem Geol 120: 275–294

Ionov DA, Hofmann AW, Shimizu N (1994) Metasomatism-induced melting in mantle xenoliths from Mongolia. J Petrol 35: 753–785

Ionov DA, Kramm U, Stosch H-G (1992b) Evolution of the upper mantle beneath the southern Baikal rift zone: a Sr–Nd isotope study of xenoliths from the Bartoy volcanoes. Contrib Mineral Petrol 111: 235–247

Jagoutz E, Wänke H (1986) Sr and Nd isotopic systematics of Shergotty meteorite. Geochim Cosmochim Acta 50: 939–953

Jaques AL, Green DH (1980) Anhydrous melting of peridotite at 0–15 Kb pressure and the genesis of tholeiitic basalts. Contrib Mineral Petrol 73: 287–310

Kiselev AI, Popov AM (1992) Asthenospheric diapir beneath the Baikal rift: petrological constraints. Tectonophysics 208: 287–295

Kiselev AI, Medvedev ME, Golovko GA (1979) Volcanism of the Baikal rift zone and problems of deep magma generation (in Russian). Nauka, Novosibirsk

Kurat G, Palme H, Embey-Isztin A, Touret J, Ntaflos T, Spettel B, Brandstätter B, Palme C, Dreibus G, Prinz M (1993) Petrology and geochemistry of peridotites and associated vein rocks of Zabargad Island, Red Sea, Egypt. Mineral Petrol 48: 309–341

Kushiro I, Yoder HS (1966) Anorthite-forsterite and anorthite-enstatic reactions and their bearing on the basalt-eclogite transformation. J Petrol 7: 337–362

Logatchev NA, Zorin YA (1987) Evidence and causes of the two-stage development of the Baikal rift. Tectonophysics 143: 225–234

McDonough WF, Stosch HG, Ware NG (1992) Distribution of titanium and the rare earth elements between peridotitic minerals. Contrib Mineral Petrol 110: 321–328

O'Reilly SY, Griffin WL (1985) A xenolith-derived geotherm for southeastern Australia and its geophysical implications. Tectonophysics 111: 41–63

O'Reilly SY, Griffin WL, Ryan CG (1991) Residence of trace elements in metasomatized spinel lherzolite xenoliths: a proton microprobe study. Contrib Mineral Petrol 109: 98–113

Piccardo GB, Messiga B, Vannucci R (1988) The Zabargad peridotite-pyroxenite association: petrological constraints on its evolution. Tectonophysics 150: 135-162

Pouchou JL, Pichoir F (1984) A new model for quantitative X-ray microanalysis. Part 1: application to the analysis of homogeneous samples. Rech Aérosp 5: 13–38

Press S, Witt G, Seck HA, Ionov DA, Kovalenko VI (1986) Spinel peridotite xenoliths from the Tariat Depression, Mongolia. I: Major element chemistry and mineralogy of a primitive mantle xenolith suite. Geochim Cosmochim Acta 50: 2587–2599

Rampone E, Bottazzi P, Ottolini L (1991) Complementary Ti−Zr anomalies in orthopyroxene and clinopyroxene in mantle peridotites. Nature 354: 518–520

Rampone E, Piccardo GB, Vannucci R, Bottazzi P, Ottolini L (1993) Subsolidus reactions monitored by trace element partitioning: the spinel- to plagioclase-facies transition in mantle peridotites. Contrib Mineral Petrol 115: 1–17

Rampone E, Hofmann AW, Piccardo GB, Vannucci R, Bottazzi P, Ottolini L (1995) Petrology, mineral and isotope geochemistry of the External Liguride peridotites (Northern Appennines, Italy). J Petrol 36: 81–105

Ryan CG, Cousens DR, Sie SH, Griffin WL, Suter GF, Clayton E (1990) Quantitative PIXE microanalysis of geological materi-

als using the CSIRO proton microprobe. Nucl Instrum Methods Phys Res B47: 55–71
Sachtleben T, Seck HA (1981) Chemical control of Al-solubility in orthopyroxene and its implications on pyroxene geothermometry. Contrib Mineral Petrol 78: 157–165
Sen G (1988) Petrogenesis of spinel lherzolite and pyroxenite suite xenoliths from the Koolau shield, Oahu, Hawaii: implications for petrology of the post-eruptive lithosphere beneath Oahu. Contrib Mineral Petrol 100: 61–91
Stosch H-G, Lugmair GW, Kovalenko VI (1986) Spinel peridotite xenoliths from the Tariat Depression, Mongolia. II: Geochemistry and Nd and Sr isotopic composition and their implications for the evolution of the subcontinental lithosphere. Geochim Cosmochim Acta 50: 2601–2614
Wells PRA (1977) Pyroxene thermometry in simple and complex systems. Contrib Mineral Petrol 62: 129–139
Wendlandt RF, Eggler DH (1980) Stability of sanidine+forsterite and its bearing on the genesis of potassic magmas and the distribution of potassium in the upper mantle. Earth Planet Sci Lett 51: 215–220
Wilshire HG, McGuire AV, Noller JS, Turrin BD (1991) Petrology of lower crustal and upper mantle xenoliths from the Cima volcanic field, California. J Petrol 32: 169–200
Windom KE, Unger CP (1988) Stability of the assemblage albite plus forsterite at high temperatures and pressures with petrologic implications. Contrib Mineral Petrol 98: 390–400
Woodland AB, Kornprobst J, Wood BJ (1992) Oxygen thermobarometry of orogenic lherzolite massifs. J Petrol 33: 203–220
Zindler A, Hart S (1986) Chemical geodynamics. Ann Rev Earth Planet Sci 14: 493–571
Zindler A, Jagoutz E (1986) Mantle cryptology. Geochim Cosmochim Acta 52: 319–333
Zorin YA, Turutanov EK, Novoselova MR, Bulk TV (1989) A three-dimentional model of the lithosphere in the southern part of Eastern Siberia. Geotectonics 23: 72–80